Optics Letters

Laser waveform control of extreme ultraviolet high harmonics from solids

Yong Sing You,[1] Mengxi Wu,[2] Yanchun Yin,[3,4] Andrew Chew,[3,4] Xiaoming Ren,[3,4] Shima Gholam-Mirzaei,[4] Dana A. Browne,[2] Michael Chini,[4] Zenghu Chang,[3,4] Kenneth J. Schafer,[2] Mette B. Gaarde,[2] and Shambhu Ghimire[1,*]

[1]Stanford PULSE Institute, SLAC National Accelerator Laboratory, Menlo Park, California 94025, USA
[2]Department of Physics and Astronomy, Louisiana State University, Baton Rouge, Louisiana 70803, USA
[3]Institute for the Frontier of Attosecond Science and Technology, CREOL and Department of Physics, University of Central Florida, Orlando, Florida 32816, USA
[4]Department of Physics, University of Central Florida, Orlando, Florida 32816, USA
*Corresponding author: shambhu@slac.stanford.edu

Received 2 February 2017; accepted 28 March 2017; posted 3 April 2017 (Doc. ID 285934); published 27 April 2017

Solid-state high-harmonic sources offer the possibility of compact, high-repetition-rate attosecond light emitters. However, the time structure of high harmonics must be characterized at the sub-cycle level. We use strong two-cycle laser pulses to directly control the time-dependent nonlinear current in single-crystal MgO, leading to the generation of extreme ultraviolet harmonics. We find that harmonics are delayed with respect to each other, yielding an atto-chirp, the value of which depends on the laser field strength. Our results provide the foundation for attosecond pulse metrology based on solid-state harmonics and a new approach to studying sub-cycle dynamics in solids.

OCIS codes: (320.7130) Ultrafast processes in condensed matter, including semiconductors; (320.7120) Ultrafast phenomena; (320.7110) Ultrafast nonlinear optics.

https://doi.org/10.1364/OL.42.001816

Attosecond pulse metrology is currently based on the generation of extreme ultraviolet (XUV) high harmonics from atoms and molecules in the gas phase [1]. The duration of isolated attosecond pulses is approaching the atomic unit of time [2], but typical gas phase harmonic sources do not provide the photon flux desired for many applications. Harmonic sources based on solid targets are emerging as promising candidates because of their high efficiency and modest requirements for the driving laser peak intensity [3–6], making them particularly compatible with the use of high-repetition-rate pump lasers [7]. However, applications in attosecond metrology require sources with precisely characterized and controllable time-frequency profiles, and a robust experimental method that can both probe and control the dynamics directly in the time domain is therefore essential to unlocking the potential of solid-state high-order harmonic generation (HHG) sources.

Gas-phase attosecond sources exhibit an intrinsic chirp at the sub-cycle level, meaning that different XUV harmonics are emitted at different times within the optical cycle [8]. This so-called atto-chirp originates in the microscopic generation process and can be understood within the recollision model for the gas phase HHG [9]. The solid-state HHG mechanism is fundamentally different as evidenced by the field dependence of the maximum photon energy produced [10], its complex ellipticity dependence [6], and the emergence of multiple plateau structures in the harmonic spectrum [4]. Two microscopic mechanisms, based on intraband and interband nonlinear currents, have been proposed to explain the HHG process in solids [10,11], and elucidating their relative importance is currently a matter of intense debate [3,12–17]. It is predicted that the radiation from the nonlinear interband current exhibits atto-chirp, whereas that resulting from intraband Bloch oscillations does not [15]. Therefore, the measurement of the atto-chirp of solid-state harmonics could confirm the microscopic generation mechanism.

In this Letter, we probe the intrinsic atto-chirp of high-order harmonics from single-crystal MgO by observing how the XUV spectrum changes under different carrier envelope phase (CEP) settings of the driving laser pulse. We use waveform-controlled two-cycle laser pulses to produce high-order harmonics in the XUV spectral range. The measured harmonic spectrum shows strong sensitivity to the CEP of the laser pulse such that the harmonic peaks shift significantly by more than the laser photon energy when the CEP is changed by π. We reproduce the measured spectra and their CEP dependence in calculations by solving the time-dependent Schrodinger equation (TDSE) for a strongly driven three-level system that originates in the band structure at the high symmetry (Γ) point. Our results indicate that the large CEP shift originates in the atto-chirp of the harmonic radiation, consistent with the HHG process being dominated by interband contributions [11,15,16,18].

In our experiments, we focus two-cycle laser pulses with a 1.7 μm central wavelength obtained from an optical parametric

chirped-pulse amplifier system [19] into a 001-cut 200 μm thick MgO crystal. We estimate the field strength inside the crystal to be ~2 V/Å (peak intensity ~10^{14} W/cm^2), which is just below the damage threshold at a repetition rate of 1 kHz. Such a relatively high damage threshold is reached due to the relatively large bandgap (7.8 eV), small photon energy (0.73 eV), and ultra-short pulse duration (~11 fs). The laser polarization is along the cubic direction where the conversion efficiency is highest [6]. High harmonics emitted in transmission are analyzed using an XUV spectrometer consisting of a flat-field variable groove density grating and a micro-channel plate detector. Figure 1(a) shows representative measured spectra at two different CEP settings with an offset of $\pi/2$. The setting on the left produces fairly discrete harmonic peaks in the primary plateau, indicating that at least two XUV bursts were emitted with approximately half-cycle periodicity, while the setting on the right produces a more continuous plateau suggesting that the XUV emission occurred in a dominant single burst. The secondary plateau visible in both plots is much weaker, but also exhibits some dependence on the CEP.

To calculate the high-harmonic spectrum, we solve TDSE for a strongly driven three-level system that originates in the band structure of MgO at the high symmetry Γ point, as shown in Fig. 1(b). The band structure and transition matrix elements are calculated via density functional theory (DFT), using the Perdew–Burke–Ernzeroff GGA functional [20] and employing the linear augmented plane wave plus local orbital basis as implemented in the WIEN2k software package [21]. The calculations use a muffin tin radius of 1.98 Bohr for both Mg and O, a k-point grid of 20 × 20 × 20 in the Brillouin zone, and a plane wave cutoff of 32 a.u. Since standard DFT calculations produce an energy gap that is smaller than the experimental value, the conduction band energies are shifted to get better agreement with the experimental band structure. When driven by linearly polarized light, the three bands that predominantly contribute to the harmonic spectra are VB, CB1, and CB2, which have energies at 0, 7.8, and 24.6 eV at the Γ point. The only non-zero transition matrix elements are μVB-CB1 = 0.33 a.u. and μVB-CB2 = 0.65 a.u.. The higher bands contribute significantly only at higher driving fields and at energies in the vicinity of (and above) the VB-CB2 bandgap. The interference between the contributions from the lower and higher-lying conduction bands gives rise to the minimum in the calculated harmonic spectra [most clearly seen in Fig. 2(f)]. To model the fast dephasing time, we have introduced a quarter-cycle dephasing time in the calculation [11].

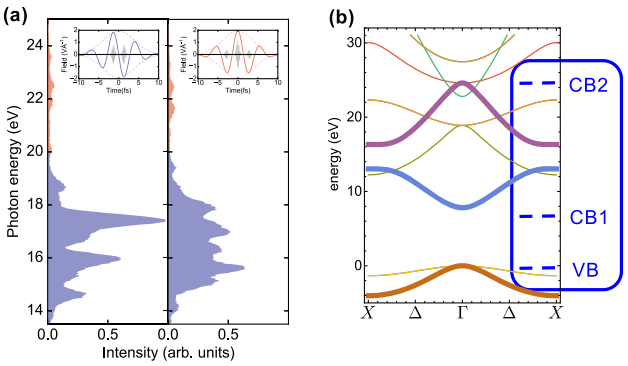

Fig. 1. Intense two-cycle laser pulses are focused into a 200 μm thick MgO crystal to produce high harmonics. The harmonic spectrum is sensitive to the CEP of the drive laser; for example, (a) shows representative measured spectra for a sine-like and a cosine-like pulse as shown in the insets. The estimated peak field strength inside the sample is ~2 V/Å. Both spectra contain a primary (blue) and a much weaker secondary plateau (red), in total extending to around 25 eV. The insets illustrate XUV bursts generated every half-cycle of the laser pulse such that their relative strengths depend on the CEP. The sine-like pulse, with two equal half-cycles, would produce a spectrum with discrete harmonic peaks while a cosine-like pulse with a single, main half-cycle would produce a near continuous plateau. (b) shows a portion of the band structure of MgO obtained from DFT calculations. The three major bands (VB, CB1, and CB2) that contribute to HHG are shown with solid lines. The inset shows their energy levels at the Γ point.

The waveform manipulation of the harmonic spectrum is demonstrated in Fig. 2. The top row [Figs. 2(a)–2(c)] shows the measured CEP dependence for the different field strengths of ~1.2 V/Å, 1.7 V/Å, and 2.1 V/Å, respectively. In all the measurements, we observe that when the CEP is increased, the harmonic peaks shift toward higher photon energy, forming a slope of photon energy versus the CEP (indicated by the black dashed line in the figures). As seen in Fig. 2(a), for a peak field of 1.2 V/Å, the CEP slope around 18 eV is about 1.7 eV/Å. At higher peak fields ((b) and (c)), the slopes are 0.8 eV/π and 0.7 eV/π, respectively; i.e., the slope for the same harmonic decreases with the increase of laser field strength. This behavior is well reproduced in the calculations [bottom row, Figs. 2(d)–2(f)], with slopes of 1.4 eV/π, 0.5 eV/π, and 0.3 eV/π for 1.0 V/Å, 1.3 V/Å, and 1.8 V/Å, respectively (calculations were performed using a 1.6 μm central wavelength). In the calculations, we also observe that, for a given field strength, the CEP slope increases with the harmonic order, from being very flat deep in the plateau to much steeper near the cutoff. For field strengths ~1.7 V/Å and above, we observe a minimum in the spectrum around 20 eV and a secondary plateau that extends to higher energies. This is similar to the recent observation of a secondary plateau in rare gas solids, originating in multi-band couplings [4]. We note that the fact that the CEP dependence persists in both plateaus means that both conduction bands are being accessed at the sub-cycle timescale.

The dependence of the harmonic frequencies on the CEP implies that in our experiment the bursts of XUV light emitted in consecutive half-cycles are not identical in terms of their spectral content and their spectral phase. This is in contrast to the harmonic emission from a typical multi-cycle laser pulse in which the interference between identical pulses with half-cycle temporal spacing gives rise to the well-known spectrum consisting of odd harmonic peaks. For a two-cycle pulse, the burst-to-burst difference originates in the sub-cycle emission dynamics in the solid, which depends on the instantaneous value of the laser vector potential [15,22].

The emission dynamics are illustrated in Fig. 3(a), which shows the calculated time-frequency profile for a field strength of 1.0 V/Å and a CEP of zero. The photon energies between approximately 8 and 20 eV are emitted in three to four short bursts, each exhibiting a rapid frequency chirp, with higher energies emitted later than lower energies. In our model, the above bandgap (VB-CB) emission pattern can be understood in terms of interband coherences between the bands in the presence of the laser field. For a two-level system, the instantaneous energy difference between the field-dressed states is given by

$$\varepsilon(t) = 2\sqrt{(\mu A(t))^2 + (\omega_0/2)^2}, \quad (1)$$

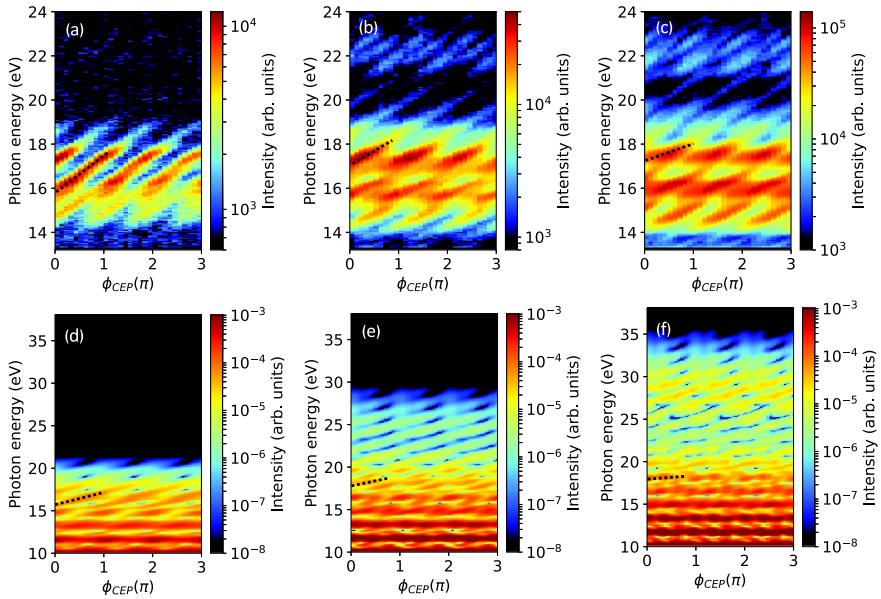

Fig. 2. Top row shows the measured CEP dependence of HHG from MgO with peak laser fields of (a) 1.2 V/Å, (b) 1.7 V/Å, and (c) 2.1 V/Å, respectively. The bottom row shows calculation results from the three-level model, at similar field strengths of (d) 1.0 V/Å, (e) 1.3 V/Å, and (f) 1.8 V/Å, respectively. The dashed black lines trace the change in photon energy of the harmonic peak around 18 eV. The slope of this line for a given plateau harmonic decreases with an increasing peak field. In the calculations, which show a larger range of photon energies, this behavior can also be recognized in the CEP dependence for each intensity: the slope is largest for the highest photon energies close to the cutoff and decreases with harmonic order.

where μ is the transition matrix element, $A(t)$ is the time-dependent vector potential, and ω_0 is the bandgap. Harmonics are emitted when the photon energy matches the instantaneous energy difference. The dashed line in Fig. 3(a) shows the instantaneous VB-CB separation $\varepsilon(t)$ for our three-level system, which is in excellent agreement with the sub-cycle XUV emission time.

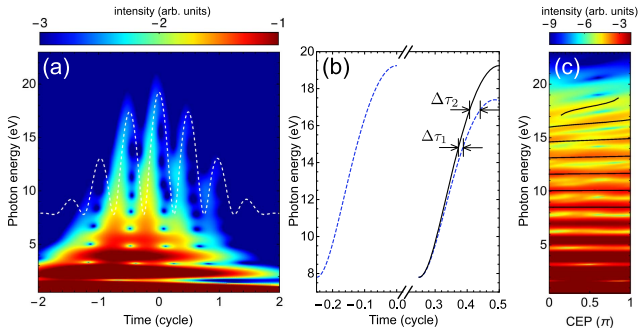

Fig. 3. (a) Calculated time-frequency profile of the HHG emission using a field strength of 1.0 V/Å and a CEP of zero. The color scale indicating the spectral yield is logarithmic. The dashed lines indicate predicted time-dependent photon energies. Photon energies above the bandgap (7.8 eV) are emitted in interband processes, which gives rise to a rapid chirp where higher energies are emitted later. (b) Zoom-in on two half-cycles of the predicted time-dependent photon energy, near the peak of the pulse. The dashed lines are the same as those in (a). The solid line is a copy of the dashed line in the first half-cycle. The emission time of a given frequency differs between the two half-cycles, and the difference depends on the photon energy. (c) Calculated corresponding CEP-dependent spectrum of HHG radiation with a field strength of 1.0 V/Å. The black lines overlaid are calculated from the interference between subsequent pulses with different phases, corresponding to different sub-cycle emission times.

The rapid sub-cycle chirp of the interband harmonics, in combination with the different maximum photon energy in each half-cycle, explains the CEP dependence observed in the experiment. This is illustrated qualitatively in Figs. 3(b) and 3(c). The dashed lines in Fig. 3(b) show the predicted time-dependent photon energy of two of the sub-cycle bursts in Fig. 3(a) and, for comparison, the solid line in the second half-cycle is a copy of the first burst, translated by exactly one half-cycle. It is clear from the figure that the emission time of a given energy changes from half-cycle to half-cycle. For the two half-cycles shown, the repetition time is slightly more than one half-cycle, and changes with photon energy. In the spectral domain, this will give rise to peaks that are separated by slightly less than twice the laser frequency, and the separation will change with photon energy.

This understanding can be formalized by considering the interference between two adjacent XUV bursts. The XUV bursts generated in each half-cycle have different amplitudes and phases that depend on the instantaneous intensity and the CEP, which can lead to constructive or destructive interference [23]. Consider the time-dependent dipole of two adjacent bursts:

$$\begin{aligned} D(t) &= d_1(t) + d_2(t) \\ &= d(t) + d(t - T/2)\exp(i(\pi + \theta_{12})), \end{aligned} \tag{2}$$

where $d(t)$ is the dipole from a single attosecond burst, and θ_{12} is the phase difference between these two attosecond bursts. We have ignored the amplitude change and consider only the phase difference, which can be written as

$$\theta_{12} = \int_{t_1}^{t_{r1}} (\varepsilon(t) - \omega_0)\mathrm{d}t - \int_{t_2}^{t_{r2}} (\varepsilon(t) - \omega_0)\mathrm{d}t, \tag{3}$$

where t_i and t_{ri} are the time of tunneling and the time when frequency ω is generated, respectively. $\varepsilon(t)$ is the time-dependent

energy difference between the first and second instantaneous eigenstates of the three-level system [dashed lines in Fig. 3(b)]. Constructive interference requires that the frequencies peak at the values given by the following equation:

$$\omega/\omega_L = 2n - 1 - \theta_{12}/\pi, \quad (4)$$

where ω_L is the laser frequency, and θ_{12} is the energy-dependent phase difference between the two bursts. $\theta_{12} = 0$ implies that the peaks occur at the odd harmonics of the driving laser. As the CEP is changed, the XUV bursts will shift under an overall envelope, leading to different emission times and, therefore, a change of θ_{12}, giving rise to the CEP pattern in Fig. 3(c). The black lines overlaid on the CEP dependence in Fig. 3(c) have been calculated using Eq. (4). The steeper CEP slope for the higher harmonics can be understood in terms of the larger burst-to-burst variation of their emission time, as seen in Fig. 3(b). Likewise, the decrease of the CEP slope of a given harmonic with field strength can be understood in terms of that harmonic moving further away from the cutoff as the field increases. We note that for harmonics below the bandgap which, in this model, originate in intraband dynamics, do not exhibit a frequency chirp, but are emitted all at the same time each half-cycle [15], similar to recent time domain measurements of terahertz-driven below bandgap harmonics in GaSe [12].

We demonstrate laser-waveform control of sub-cycle dynamics that leads to the generation of XUV harmonics in single-crystal MgO subjected to two-cycle pulses with maximum field strengths ~2 V/Å. We measure significant CEP shifts ~1.7 eV/π that are comparable to those of gas phase harmonic sources [23]. The CEP shift originates in the delay between different harmonics, which indicates that the HHG mechanism in MgO is dominated by interband processes. This result is in significant contrast to the results of Hohenleutner *et al.* on GaSe [12] and of Garg *et al.* on SiO_2 [13] in which the harmonic exhibited essentially no atto-chirp—consistent with the generation from an intraband current. As MgO is an ionic solid, while GaSe and SiO_2 are covalent, the differences in atto-chirp under similar laser conditions would suggest that the nature of bonding between atomic components in a solid plays a defining role in the dynamics responsible for HHG. In our results, the CEP variation of the secondary plateau that appears at high field strengths furthermore indicates the potential for sub-cycle control of electron dynamics in multiple conduction bands. Thus analysis of the time structure of the XUV light reveals the novel underlying electron dynamics present in strongly driven solids [24–28]. In conclusion, our results provide the foundation for attosecond pulse metrology based on solid-state HHG along with implications in petahertz electronics based on ultrafast laser driven multi-band electron dynamics.

Funding. Stanford/SLAC: U.S. Department of Energy (DOE); Office of Science (SC); Basic Energy Sciences (BES), Chemical Sciences, Geosciences, and Biosciences Division through the Early Career Research Program; LSU and UCF: National Science Foundation (NSF) (PHY-1403236, PHY-1506345); UCF: Air Force Office of Scientific Research (AFOSR) (FA9550-15-1-0037, FA9550-16-1-0149); Army Research Office (ARO) (W911NF-14-1-0383, W911NF-15-1-0336); Defense Advanced Research Projects Agency (DARPA) PULSE Program (AMRDEC W31P4Q1310017).

Acknowledgment. S. G. and Y. S. Y. thank David Reis for fruitful discussions.

REFERENCES

1. P. B. Corkum and F. Krausz, Nat. Phys. **3**, 381 (2007).
2. K. Zhao, Q. Zhang, M. Chini, Y. Wu, X. Wang, and Z. Chang, Opt. Lett. **37**, 3891 (2012).
3. T. T. Luu, M. Garg, S. Y. Kruchinin, A. Moulet, M. T. Hassan, and E. Goulielmakis, Nature **521**, 498 (2015).
4. G. Ndabashimiye, S. Ghimire, M. Wu, D. A. Browne, K. J. Schafer, M. B. Gaarde, and D. A. Reis, Nature **534**, 520 (2016).
5. H. Liu, Y. Li, Y. S. You, S. Ghimire, T. F. Heinz, and D. A. Reis, Nat. Phys. **13**, 262 (2016).
6. Y. S. You, D. A. Reis, and S. Ghimire, Nat. Phys. **13**, 345 (2016).
7. M. Krebs, S. Hädrich, S. Demmler, J. Rothhardt, A. Zaïr, L. Chipperfield, J. Limpert, and A. Tünnermann, Nat. Photonics **7**, 555 (2013).
8. Y. Mairesse, A. D. Bohan, L. J. Frasinski, H. Merdji, L. C. Dinu, P. Monchicourt, P. Breger, M. Kovačev, R. Taïeb, B. Carré, H. G. Muller, P. Agostini, and P. Salières, Science **302**, 1540 (2003).
9. P. Corkum, Phys. Rev. Lett. **71**, 1994 (1993).
10. S. Ghimire, A. D. DiChiara, E. Sistrunk, P. Agostini, L. F. DiMauro, and D. A. Reis, Nat. Phys. **7**, 138 (2011).
11. G. Vampa, C. McDonald, G. Orlando, D. Klug, P. Corkum, and T. Brabec, Phys. Rev. Lett. **113**, 073901 (2014).
12. M. Hohenleutner, F. Langer, O. Schubert, M. Knorr, U. Huttner, S. W. Koch, M. Kira, and R. Huber, Nature **523**, 572 (2015).
13. M. Garg, M. Zhan, T. T. Luu, H. Lakhotia, T. Klostermann, A. Guggenmos, and E. Goulielmakis, Nature **538**, 359 (2016).
14. S. Ghimire, A. D. DiChiara, E. Sistrunk, G. Ndabashimiye, U. B. Szafruga, A. Mohammad, P. Agostini, L. F. DiMauro, and D. A. Reis, Phys. Rev. A **85**, 043836 (2012).
15. M. Wu, S. Ghimire, D. A. Reis, K. J. Schafer, and M. B. Gaarde, Phys. Rev. A **91**, 043839 (2015)..
16. T. Higuchi, M. I. Stockman, and P. Hommelhoff, Phys. Rev. Lett. **113**, 213901 (2014).
17. P. G. Hawkins, M. Y. Ivanov, and V. S. Yakovlev, Phys. Rev. A **91**, 013405 (2015).
18. G. Vampa, T. J. Hammond, N. Thiré, B. E. Schmidt, F. Légaré, C. R. McDonald, T. Brabec, and P. B. Corkum, Nature **522**, 462 (2015).
19. Y. Yin, J. Li, X. Ren, K. Zhao, Y. Wu, E. Cunningham, and Z. Chang, Opt. Lett. **41**, 1142 (2016).
20. J. P. Perdew, K. Burke, and M. Ernzerhof, Phys. Rev. Lett. **77**, 3865 (1996).
21. P. Blaha, K. Schwarz, G. Madsen, D. Kvasnicka, and J. Luitz, *WIEN2K, An Augmented Plane Wave + Local Orbitals Program for Calculating Crystal Properties* (Karlheinz Schwarz, Techn. Universität Wien, Austria, 2001).
22. M. Wu, D. A. Browne, K. J. Schafer, and M. B. Gaarde, Phys. Rev. A **94**, 063403 (2016).
23. A. Y. Naumov, D. M. Villeneuve, and H. Niikura, Phys. Rev. A **91**, 063421 (2015).
24. A. Schiffrin, T. Paasch-Colberg, N. Karpowicz, V. Apalkov, D. Gerster, S. Mühlbrandt, M. Korbman, J. Reichert, M. Schultze, S. Holzner, J. V. Barth, R. Kienberger, R. Ernstorfer, V. S. Yakovlev, M. I. Stockman, and F. Krausz, Nature **493**, 70 (2013).
25. M. Schultze, K. Ramasesha, C. D. Pemmaraju, S. A. Sato, D. Whitmore, A. Gandman, J. S. Prell, L. J. Borja, D. Prendergast, K. Yabana, D. M. Neumark, and S. R. Leone, Science **346**, 1348 (2014).
26. A. Sommer, E. M. Bothschafter, S. A. Sato, C. Jakubeit, T. Latka, O. Razskazovskaya, H. Fattahi, M. Jobst, W. Schweinberger, V. Shirvanyan, V. S. Yakovlev, R. Kienberger, K. Yabana, N. Karpowicz, M. Schultze, and F. Krausz, Nature **534**, 86 (2016).
27. H. Mashiko, K. Oguri, T. Yamaguchi, A. Suda, and H. Gotoh, Nat. Phys. **12**, 741 (2016).
28. O. Kwon, T. Paasch-Colberg, V. Apalkov, B.-K. Kim, J.-J. Kim, M. I. Stockman, and D. Kim, Sci. Rep. **6**, 21272 (2016).